# The Bispecific Tumor Antigen-Conditional 4–1BB x 5T4 Agonist, ALG.APV-527, Mediates Strong T-Cell Activation and Potent Antitumor Activity in Preclinical Studies

Michelle H. Nelson[1], Sara Fritzell[2], Robert Miller[1], Doreen Werchau[2], Danielle Van Citters[1], Anneli Nilsson[2], Lynda Misher[1], Lill Ljung[2], Robert Bader[1], Adnan Deronic[2], Allison G. Chunyk[1], Lena Schultz[2], Laura A. Varas[2], Nadia Rose[3], Maria Håkansson[3], Jane Gross[1], Christina Furebring[2], Peter Pavlik[1], Anette Sundstedt[2], Niina Veitonmäki[2], Hilario J. Ramos[1], Anna Säll[2], Anna Dahlman[2], David Bienvenue[1], Laura von Schantz[2], Catherine J. McMahan[1], Maria Askmyr[2], Gabriela Hernandez-Hoyos[1], and Peter Ellmark[2,4]

## ABSTRACT

4–1BB (CD137) is an activation-induced costimulatory receptor that regulates immune responses of activated CD8 T and natural killer cells, by enhancing proliferation, survival, cytolytic activity, and IFNγ production. The ability to induce potent antitumor activity by stimulating 4–1BB on tumor-specific cytotoxic T cells makes 4–1BB an attractive target for designing novel immuno-oncology therapeutics. To minimize systemic immune toxicities and enhance activity at the tumor site, we have developed a novel bispecific antibody that stimulates 4–1BB function when co-engaged with the tumor-associated antigen 5T4. ALG.APV-527 was built on the basis of the ADAPTIR bispecific platform with optimized binding domains to 4–1BB and 5T4 originating from the ALLIGATOR-GOLD human single-chain variable fragment library. The epitope of ALG.APV-527 was determined to be located at domain 1 and 2 on 4–1BB using X-ray crystallography. As shown in reporter and primary cell assays *in vitro*, ALG.APV-527 triggers dose-dependent 4–1BB activity mediated only by 5T4 cross-linking. *In vivo*, ALG.APV-527 demonstrates robust antitumor responses, by inhibiting growth of established tumors expressing human 5T4 followed by a long-lasting memory immune response. ALG.APV-527 has an antibody-like half-life in cynomolgus macaques and was well tolerated at 50.5 mg/kg. ALG.APV-527 is uniquely designed for 5T4-conditional 4–1BB–mediated antitumor activity with potential to minimize systemic immune activation and hepatotoxicity while providing efficacious tumor-specific responses in a range of 5T4-expressing tumor indications as shown by robust activity in preclinical *in vitro* and *in vivo* models. On the basis of the combined preclinical dataset, ALG.APV-527 has potential as a promising anticancer therapeutic for the treatment of 5T4-expressing tumors.

## Introduction

Checkpoint inhibitor treatment has revolutionized cancer treatment resulting in sustainable clinical benefit. However, not all patients respond to this type of therapy, and there is need for additional improvements. A promising approach for cancer immunotherapy is to activate tumor-infiltrating T cells and natural killer (NK) cells through 4–1BB costimulation using antigen-conditional 4–1BB agonists (1).

4–1BB (TNF receptor superfamily 9, TNFRSF9, CD137) is a costimulatory receptor transiently expressed on various immune cells such as activated CD8 cytotoxic T cells, CD4 helper T cells, B cells, regulatory T cells, NK cells, natural killer T cells, and different myeloid cell populations (2). 4–1BB ligation provides the immune cell with a costimulatory signal that activates intracellular signaling cascades, for example, the NFκB pathway, inducing an increase in proliferation, cytokine production, and cytolytic activity (3, 4), and promoting T-cell survival and long-term protection from tumor recurrence (5). Although 4–1BB expression is low in naïve peripheral T cells, 4–1BB is highly upregulated upon T-cell receptor (TCR) activation on tumor-infiltrating T cells capable of killing tumor cells (6–9). In the immunosuppressive tumor microenvironment (TME), there is often a lack of costimulatory signals, such as the 4–1BB ligand (4–1BBL), limiting T-cell activation (10). Therefore, therapeutic antibodies targeting 4–1BB have been developed to mimic 4–1BBL stimulation to promote more effective antitumor responses. Although most 4–1BB agonistic mAbs require clustering via Fcγ receptors (FcγR) to activate 4–1BB, bispecific antibodies (bsAbs) use binding to antigens expressed in the TME to induce clustering and 4–1BB activation.

5T4 (trophoblast glycoprotein) is an oncofetal tumor-associated antigen (TAA) expressed in embryogenic trophoblasts. In adults, 5T4 has limited normal tissue expression restricted to some specialized

[1]Aptevo Therapeutics Inc., Seattle, Washington. [2]Alligator Bioscience AB, Lund, Sweden. [3]Saromics Biostructures AB, Lund, Sweden. [4]Department of Immunotechnology, Lund University, Lund, Sweden.

G. Hernandez-Hoyos and P. Ellmark contributed equally as co-authors of this work.

M.H. Nelson and S. Fritzell contributed equally as co-authors of this work.

**Corresponding Author:** Peter Ellmark, Alligator Bioscience, Medicon Village, 223 81 Lund, Sweden. Phone: 467-9721-2739; E-mail: pek@alligatorbioscience.com

Mol Cancer Ther 2023;22:89–101

**doi:** 10.1158/1535-7163.MCT-22-0395

epithelium. In contrast, 5T4 is expressed on numerous solid tumor malignancies, including mesothelioma, non–small cell lung carcinoma (NSCLC), breast, head and neck, cervical, renal, gastric, and colorectal cancer (11–15). 5T4 is also highly expressed on tumor-initiating stem-cell–like cells (16).

We have developed ALG.APV-527, a novel 4–1BB x 5T4-targeting bsAb, to overcome limitations of the first generation of 4–1BB-targeting agonist mAbs, which elicited either on-target crosslinking-independent hepatotoxicity (17) or low potency due to a combination of weak agonistic function and poor FcγR crosslinking (18). By targeting a TAA, ALG.APV-527 has the potential for improved tumor-directed efficacy over mAbs. ALG.APV-527 is designed to activate 4–1BB on T and NK cells only when simultaneously bound to 5T4-expressing tumor cells. ALG.APV-527 has been engineered with point mutations to reduce FcγR interactions to ensure 5T4-dependent crosslinking, resulting in 5T4-conditional 4–1BB activation at sites where both targets are expressed. Because 5T4 expression is highly enriched in tumor compared with healthy tissue (11–15), and 4–1BB expression is primarily inducible by recent TCR or cytokine stimulation on activated immune cells (6–9), the overlapping expression pattern of both targets is expected to restrict immune activation by ALG.APV-527 to the TME. Thus, ALG.APV-527 has the potential to enhance antitumoral T-cell responses in a highly specific and targeted manner.

## Materials and Methods

### Cell lines and primary cells

All cell lines were cultured according to the supplier's instructions. Chinese hamster ovary (CHO-K1) cell lines were generated with stable expression of human or cynomolgus 4–1BB, human or cynomolgus 5T4 or human FcγRs. CHO cells transfected with an empty vector served as negative control.

The Jurkat T-cell line was genetically engineered in-house to express both human 4–1BB and a luciferase reporter driven by NFκB to generate a reporter cell line to assess the potency of 4–1BB agonism.

CT26 wild-type (WT) cells (CT26.WT, ATCC) were transfected with human 5T4 and single-cell clones expressing either high, intermediate or low levels of human 5T4 were sorted using flow cytometry (referred to as CT26-hu5T4 or CT26-hu5T4$^{high}$, CT26-hu5T4$^{intermediate}$ and CT26-hu5T4$^{low}$). The MB49 murine bladder carcinoma (EMD Millipore) was also transfected to express human 5T4 (MB49-hu5T4). HCT 116 and B16-F10.WT cells were obtained at ATCC. B16-F10 cells expressing human 5T4 (B16-hu5T4), was kindly provided by Prof. Peter Stern (Immunology, Division of Molecular & Clinical Cancer Sciences, University of Manchester, UK). All 5T4$^{+}$ cell lines were characterized for their 5T4 expression using a receptor density kit (α-human IgG Quantum Simply Cellular or BD Quantibrite beads).

Cell lines used herein were purchased and tested for *Mycoplasma* between 2012 and 2019, authenticated by the vendor, and used within 10 weeks of culture (up to 20 passages).

Human primary peripheral blood mononuclear cells (PBMCs) were enriched from leucocyte concentrates obtained from healthy donors. Cynomolgus PBMCs were isolated from whole blood (Silabe) using Lympholyte Mammal Cell Separation Media (Cedarlane Labs). Human CD8 T cells were enriched from PBMCs by negative selection using a MACS CD8$^{+}$ T-cell isolation kit (Miltenyi). NK cells were isolated from PBMC by negative selection using EasySep Human NK Cell Isolation Kit (Stemcell) according to EasyStep protocol and then prestimulated with 8–10 ng/mL of IL2 (Peprotech) overnight in 37°C. No patient samples were used in these studies.

### ALG.APV-527 molecular design, lead selection, and optimization

The parental 5T4 and 4–1BB–targeting binding domains were obtained from the human single-chain (scFv, single-chain variable fragment) antibody library ALLIGATOR-GOLD. Following several phage selection strategies directed against the two targets, specific binders were identified and screened as soluble scFv or phages by ELISA and flow cytometry. Clones that met binding, functional, and stability criteria were further evaluated in a bispecific Morrison (mAb-scFv) format.

Preferred α-4–1BB and α-5T4–binding domains were successfully incorporated into the ADAPTIR bispecific format and optimized for stability and function using random mutagenesis to identify beneficial changes to the complementarity-determining regions (CDRs) and framework regions.

Mutations to eliminate FcγR and complement binding were introduced in the immunoglobulin (IgG) 1 Fc region. These consisted of the LALA mutations at L234A and L235A, along with mutations G237A and K322A according to EU numbering.

ALG.APV-527 (WO 2019/016402, SEQ ID NO: 174) was expressed by transient transfection of ExpiCHO-S cells or from a stable Freedom CHO-S cell line (Gibco/Thermo Fisher Scientific) and purified by MabSuRe Protein A and size-exclusion chromatography. ALG.APV-527 was biotinylated using the EZ-Link Sulfo-NHS-LC-Biotin kit. Urelumab analogue was produced by transient transfection of ExpiCHO-S based on the primary protein sequence of the Fab domain (19).

ALG.APV-527 was evaluated for binding to CHO-FcγR cells using α-huIgG-Fc secondary Ab and analyzed by flow cytometry and FlowJo and graphed in GraphPad Prism (RRID:SCR_002798). For binding to FcγRs or FcRn, ALG.APV-527 containing WT IgG1 Fc served as positive control. An α-GFP isotype control or germlined scFv ADAPTIR control, served as negative controls in binding and functional assays.

SPR-binding studies of FcγR and huFcRn/β2M to ALG.APV-527 were conducted on a Biacore T200 system and analyzed with GE Biacore T200 Evaluation software, globally fitting data to derive kinetic parameters. All sensorgrams were fitted using a two-state reaction model. Recombinant FcRn/β2M protein and 5T4-Fc antigen, Fc-fused recombinant extracellular domain (ECD) of 5T4, were produced in-house.

### Epitope mapping and ligand blocking

A crystal structure of the complex between 4–1BB and the parental α-4–1BB Fab binding domain (Fab1618) of ALG.APV-527 structure was determined to 2.31 Å and has been deposited in the protein data bank with pdb code 7YXU. The structure was used to make a detailed epitope analysis of 4–1BB as well as a paratope analysis of Fab1618 (Supplementary Material S1—X-ray crystallography). For 4–1BB domain mapping, loss of binding of the nonoptimized parental clones of the 4–1BB–binding domains in mAb formats was investigated using a panel of human/mouse chimeric 4–1BB constructs. The 4–1BB–binding domain was tested for ligand blocking using flow cytometry (Supplementary Material S2).

### Binding to targets and target expression

SPR-binding affinity of ALG.APV-527 to recombinant, soluble human 4–1BB ectodomain was performed on a Biacore T200

system. The Biacore evaluation software was used to derive binding kinetics parameters from a 1:1 binding model fit of double-subtracted sensorgrams.

Binding ($EC_{50}$) of ALG.APV-527 to 5T4-expressing tumor cell lines and 5T4 or 4–1BB (human and cynomolgus) expressed on CHO cells was assessed by measuring the mean fluorescence intensity using flow cytometry (FACSVerse, FACSymphony or BD LSRII) via a secondary antibody, $F(ab')_2$ goat α-human IgG Fc (Jackson Immunoresearch) or Streptavidin (BD Pharmingen) and analyzed using FlowJo software (RRID:SCR_008520). To determine the number of antigens on the cell surface [measured as antibodies per cell (ABC)], BD Quantibright Beads were used. The standardized beads comprise four known values of PE to calibrate the FL2 axis and were used in conjunction with PE-bound mAb specific for the target antigen.

Binding ($EC_{50}$) of ALG.APV-527 to human 4–1BB on activated primary immune cells was assessed on freshly isolated human and cynomolgus PBMCs, incubated at 37°C with or without plate-coated CD3 stimulation (10 μg/mL α-huCD3 or 3 μg/mL α-monkey CD3) for 48 hours. Cells were then Fc-blocked (Beriglobin, huIgG, 200 μg/mL) and incubated with serially diluted biotinylated ALG.APV-527 or negative control. Following washing, cells were incubated with a secondary antibody streptavidin-APC and fluorescent-conjugated antibodies [CD4-FITC (L200), CD3-PECy7 (SP34–2), CD8-APC-H7 (SK1)] and fixable viability stain 510 (BD Pharmingen). Cells were analyzed for binding using flow cytometry by gating on viable, single cells expressing CD3 and CD8.

For IHC detection of 5T4 expression in human and cynomolgus tissue, two α-5T4 antibodies [Mouse α-5T4 (524731, R&D Systems) and rabbit α-5T4 antibody (EPR5529, Abcam)] were used. As a negative control, the detection antibodies were substituted with a mouse (MOPC-21, BD Pharmingen) and a rabbit IgG1 antibody (SP137, Abcam) that had different antigenic specificities from that of the detection antibodies (for methodology details, see Supplementary Material S3; IHC).

### Reporter assay and *in vitro* functional activity

Jurkat/4–1BB transfectants carrying a luciferase reporter gene under the control of an NFκB promoter were cultured with NCI-H1975, TF-1, MDA-MB-231 (ATCC), CHO-hu5T4, CHO-EV cells, or CHO-FcγRI (CD64), at a 1:2 reporter/target cell ratio and incubated at 37°C for 5 hours. Bio-Glo Assay Reagent (Promega) was added and incubated for 10 minutes before measuring luminescence on a MicroBeta$^2$ 2450 Microplate Counter (PerkinElmer). Potency ($EC_{50}$) values were determined using nonlinear regression analysis.

For human CD8 T-cell/tumor cell coculture assays, CT26 cells were sublethally UV irradiated using a UVB crosslinker (AnalytikJena, Lamp: 254 nm before being plated overnight; $2\times10^5$ tumor cells/well). Alternatively, for human CD8 T-cell and NK cell assays, HCT 116 cells were incubated with mitomycin C (50 μg/mL, 37°C, 45 minutes) before being plated overnight ($5\times10^5$ cells for T-cell assay; $1\times10^5$ cells for NK cell assay). The following day, serial dilutions of ALG.APV-527 were incubated with tumor cells at 37°C for 30 minutes. For T-cell cultures, addition of soluble α-CD3–coated beads at a 1:1 cell/bead ratio was followed by the addition of $1\times10^5$ unstimulated CD8 T cells. Alternatively, $2.5\times10^4$ unstimulated or IL2 prestimulated $CD56^+$ NK cells (±10 ng/mL huIL-2) were added to the tumor cells.

For human or cynomolgus CD8 T-cell assays with immobilized α-CD3 and 5T4 antigen, plates were coated overnight with α-CD3 for human cells, 3 μg/mL OKT-3; Affymetrix eBioscience or BioLegend, RRID:SCR_001134); for cynomolgus cells 1 μg/mL FN-18 (Invitrogen) and subsequently coated with 5T4-Fc antigen (5 μg/mL, 2 hours at 37°C). Assay plates were blocked with assay medium for >30 minutes. Serially diluted ALG.APV-527 was added 30 minutes before the addition of the CD8 T cells at $0.7\times10^5$/well.

For PBMC assays, two methods were used to analyze cytokine production following 72-hour incubations. Supernatant gamma IFN (IFNγ) cytokine levels were measured using the Milliplex MAP Human Cytokine/Chemokine Kit on a Luminex MagPix System. Alternatively, IFNγ levels were measured by ELISA for human IFNγ (BD OptiEIA) or cynomolgus IFNγ (Monkey IFNg ELISA, Mabtech). To determine potency, the mean of the normalized IFNγ levels from all donors (8–12) was calculated. For NK cell assays, granzyme B levels in the supernatant were tested via ELISA (Mabtech). Intracellular cytokine was measured following a 4-hour treatment with brefeldin A using flow-cytometry analysis of permeabilized cells (4S.B3; BD CytoFix/CytoPerm kit).

For proliferation assays, CHO-hu5T4 cells were irradiated for 15 minutes at 130 keV (MultiFocus, Faxitron) to prevent cell overgrowth and plated $3\times10^4$ cells/well. NK cells or PBMC were labeled with CellTrace Violet according to the manufacturer's protocol (Invitrogen). NK cells were plated at $1.2\times10^5$ cells/well with IL2 (8 ng/mL) and PBMCs were plated at $1.2\times10^5$ with α-OKT3 (10 ng/mL). Serial dilutions of ALG.APV-527 were added, and assay plates were incubated for 6 days. For cell staining, Fc-blocked cells were stained for live cells (7AAD) and surface phenotype [CD3, CD8, CD335 (9E2); BioLegend].

### Functional activity *in vivo*

Drug localization studies were conducted in accordance with guidelines provided by the Swedish Board of Agriculture and approved by the Committee of Animal Ethics in Malmö/Lund, Sweden. A B16 melanoma twin tumor model in female C57BL/6 mice (7–8 weeks; Janvier Labs) was used, where each mouse received one 5T4-negative (B16) and one 5T4-positive (B16-hu5T4) subcutaneous tumor ($1\times10^5$) on opposite sides of the flank. Intraperitoneal antibody treatments (100 μg) were given on days 13 and 15 and mice were sacrificed on day 17. To detect ALG.APV-527, tumors were snap-frozen in isopentane and stored in −80°C. Cryosections (8 μm) were acetone-fixed and blocked. Polyclonal rabbit α-human IgG (Jackson ImmunoResearch), followed by α-rabbit Brightvision–HRP (Immunologic) and DAPI were used for staining. The IHC staining was assessed: negative (0), weak staining (1+), moderate staining (2+), or strong staining (3+).

For *in vivo* efficacy experiments, female humanized 4–1BB knock-in mice (hu4–1BB KI; 7–8 weeks; Biocytogen) were used. Treatment of study animals was conducted in accordance with and under the approval of the Institutional Animal Care and Use Committee, the Guide for the Care and Use of Laboratory Animals, and the study protocol (ACUP 20). On day 0, mice were challenged subcutaneously in the hind flank with MB49-hu5T4 cells, clone 3B5 ($4 \times 10^6$). Intraperitoneal treatments were given on days 7, 10, 13, 17, 20, and 24. Body weights were monitored at least twice weekly. Tumor volume caliper measurements were done beginning on day 3 and calculated using the formula: volume $= {}^1/_2$ [length × (width)$^2$]. Tumor cells were tested for contamination by IDEXX BioAnalytics using IMACT III at passage 7 and frozen for *in vivo* use.

To examine *in vivo* systemic immune activation, Hu4–1BB KI mice with a previous curative response were tested negative for antidrug antibodies, randomized, and used 110 days post previous study. Each mouse received 200 μg of test reagent intraperitoneally on study days 0, 7, and 14. Body weights were monitored at least twice

weekly. On day 21, the final evaluation of liver, spleen, and blood was performed. Serum was taken for liver enzyme quantification by the Phoenix Laboratory. Formalin-fixed liver sections were transferred to the University of Washington, Department of Comparative Medicine and evaluated by hematoxylin and eosin and CD8 IHC by a pathologist. Splenic cells were analyzed for the quantity and proliferation (Ki67) of CD4, CD8 T cells, and NK cells via flow cytometry.

Statistical analyses were performed using SAS/JMP software (SAS Institute, RRID:SCR_008567). A repeated measures ANOVA model was fitted using Fit Model Standard Least Squares and a Tukey's post-test to evaluate overall differential effects of treatment. Differences in survival were determined using Kaplan–Meier survival analysis with a log-rank (Mantel–Cox) and Wilcoxon rank-sum tests.

To examine memory generation, mice having previously rejected MB49-hu5T4 tumors following ALG.APV-527 treatment at 180, 60 or 20 μg/mouse, were randomized and rechallenged approximately 80 days after the first tumor implantation with either MB49 or MB49-hu5T4 cells, with no additional treatment.

### Preclinical safety

For preclinical safety evaluation, cynomolgus macaques were given five, once-weekly, 1-hour intravenous doses of ALG.APV-527 (5, 15, or 50.5 mg/kg). All groups in the main study consisted of three males and three females (Supplementary Fig. S5B). In addition, a 4-week recovery period was included with two males plus two females in the control and highest-dose groups. Standard safety parameters and endpoints were evaluated. Immunophenotyping was performed on blood samples collected on days 1, 15 (pre- and 24 hours post-dose), 32, and 60. At study termination, all animals were subjected to perform a complete necropsy examination. The experiments were conducted at Charles River Laboratories, in accordance with and under the approval of the OECD Guideline 417, Committee for Medicinal Products for Human Use (CHMP) and ICH Harmonized Tripartite Guidelines M3 (R2), S3a, S7A, S7B and S9.

On days 1, 22, and 29 of the GLP toxicology study, pharmacokinetics (PKs) was evaluated in all cynomolgus macaques treated with ALG.APV-527. Blood samples were obtained at 0 (pre-dose), 5 minutes, 6, 12, 24, 48, 72, 96, and 168 hours after dosing. ALG.APV-527 serum concentration was determined via electrochemiluminescence, and data collection was performed using Discovery Workbench MesoScale Discovery. The PK parameters were estimated using Phoenix (WinNonlin) software using a noncompartmental analysis approach consistent with the intravenous infusion route of administration. Human PK simulations were performed on the basis of two-compartmental modeling from the GLP NHP toxicology study, allometrically scaled to humans.

For additional details of the preclinical safety study, PK in non-human primates (NHPs) and cytokine release assay, see Supplementary Material S4—preclinical safety.

### Data availability statement

The data generated in this study are available upon request from the corresponding author. The atomic coordinates and structure factors have been deposited in the Protein Data Bank with the primary accession code 7YXU.

## Results

### Molecular design and lead optimization of ALG.APV-527

The lead α-4–1BB and α-5T4–binding domains, obtained from the human scFv antibody library ALLIGATOR-GOLD, were incorporated into the ADAPTIR bispecific format (depicted in **Fig. 1A**) and optimized for stability, binding, and function (Supplementary Fig. S1) to meet the intended mode of action (**Fig. 1B**).

ALG.APV-527 retained binding to FcRn with an affinity of 66 nmol/L, consistent with the range of values reported for other recombinant IgG1 antibodies and other ADAPTIR bsAbs (Supplementary Fig. S2A; refs. 20, 21). The set of mutations introduced in the ADAPTIR Fc markedly reduced binding for all human and cynomolgus FcγRs tested and C1Q compared with an IgG1 WT Fc (Supplementary Fig. S2A and S2B).

### Unique binding domain of the 4–1BB parental clone of ALG.APV-527

A detailed epitope analysis, performed by X-ray crystallography using the nonoptimized parental 4–1BB–binding domain (Fab1618) showed that 4–1BB is bound mainly to the heavy chain of Fab1618 via all CDR loops (CDR1, CDR2, and CDR3; **Fig. 1C**). The interaction to the Fab1618 light chain is mostly via CDR3. The epitope on 4–1BB involves residues in domains 1 and 2 that are distinct to the 4–1BBL–binding site as well as the binding site of utomilumab and urelumab (19). Interactions include 11 hydrogen bonds out of which eight are created by amino acids situated on the heavy chain CDR loops and domain 2 on 4–1BB. A summary of the contacts and all interactions is reported in Supplementary Material S1—X-ray crystallography. A PISA (QT) analysis revealed that the interface surface area was 474.1 $Å^2$ between the Fab heavy chain and 4–1BB, including nine hydrogen bonds. The buried surface area between the Fab light chain and 4–1BB is 228.8 $Å^2$, including two hydrogen bonds.

Using a panel of human/mouse chimeric 4–1BB constructs, the crystallography data were confirmed, showing that the Fab1618 parental-binding domain depends on 4–1BB residues in the distal domains (Supplementary Material S2). Furthermore, the Fab1618 did not block 4–1BBL in binding experiments (Supplementary Material S2).

### ALG.APV-527 binds selectively to 4–1BB and 5T4

The quantity of ALG.APV-527 that binds to tumor cells is dependent on the number of 5T4 molecules expressed on the cell surface (**Fig. 2A**). The binding potency of ALG.APV-527 to CHO-expressing target cells was similar for both human and cynomolgus species (Supplementary Fig. S3A and S3B). When 5T4 binding was examined on various human and engineered cell lines, the $EC_{50}$ ranged between 8 and 20 nmol/L (Supplementary Fig. S3B). The binding affinity of ALG.APV-527 evaluated by SPR to human 4–1BB was 36 nmol/L and human 5T4 was 66 nmol/L (Supplementary Fig. S3C). Binding of ALG.APV-527 to human and cynomolgus 4–1BB expressed on primary CD8 T cells showed a similar potency to 4–1BB of both species and demonstrated that ALG.APV-527 does not bind to resting but to activated CD8 T cells (**Fig. 2B** and **C**; Supplementary Fig. S3B and S3D). In conclusion, the binding potency to 4–1BB and 5T4 from the two species is highly similar (Supplementary Fig. S3B).

5T4 expression was evaluated in both healthy and tumor tissue microarrays. 5T4 expression in normal healthy tissue was limited, and no membrane 5T4 expression was detected in any major organs, including the cardiovascular, respiratory, or hepatic systems and in line with previous reports (11–13). Importantly, 5T4 is not expressed in liver (**Fig. 2D**, 1). As expected, a strong signal for 5T4 was detected on placental trophoblasts (**Fig. 2D**, 2). 5T4 expression was also detected in multiple tumor samples, including NSCLC, mesothelioma, pancreatic cancer, and head and neck squamous cell carcinoma (**Fig. 2D**, 3–6), confirming that 5T4 is expressed on a range of tumor types.

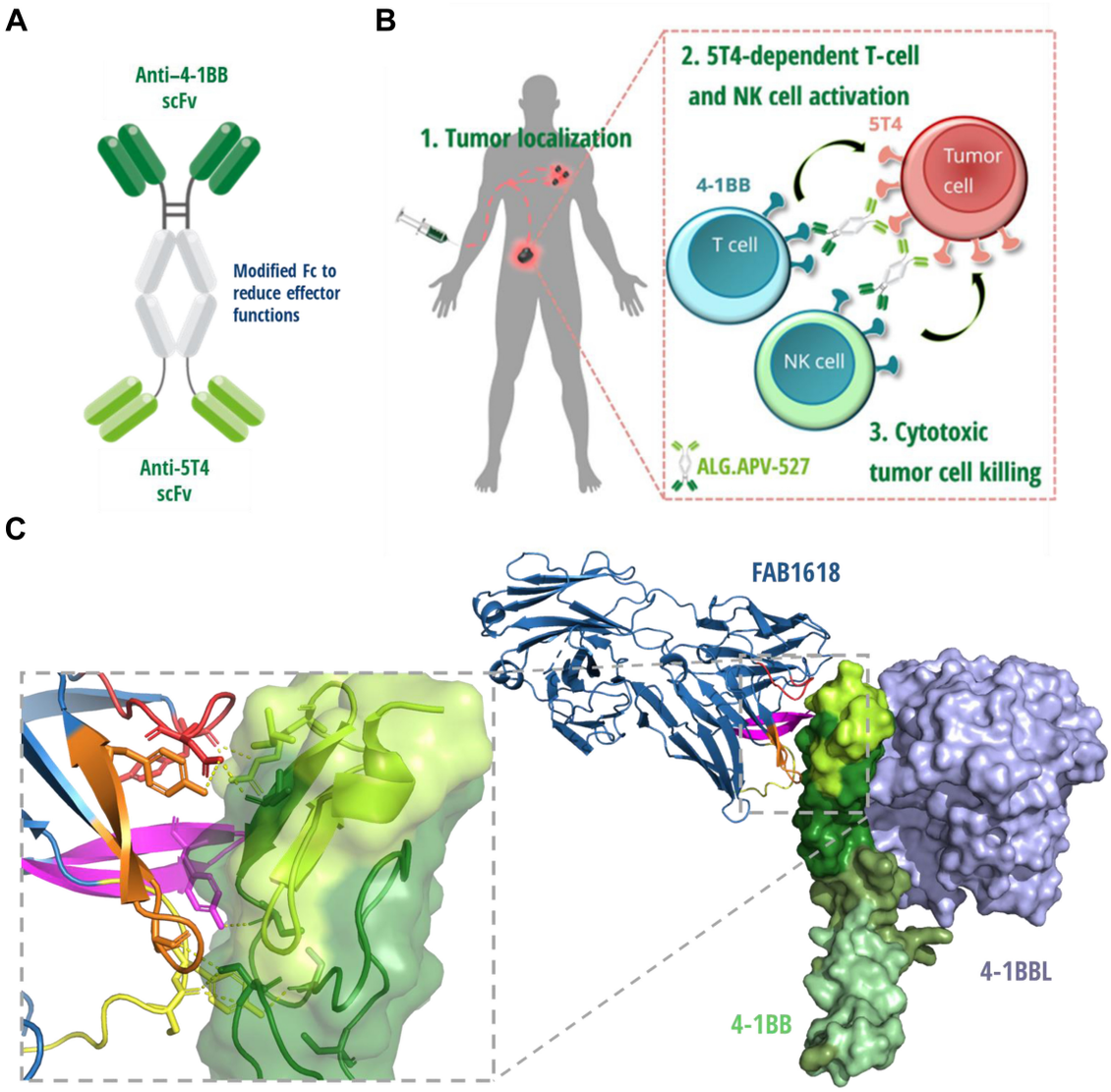


**Figure 1.**

Molecular design and optimization. **A,** ALG.APV-527 in the bispecific ADAPTIR format. ALG.APV-527 comprises two different sets of binding domains (scFv) targeting 4–1BB (shown in dark green) and 5T4 (shown in light green) linked to an IgG1 hinge and an IgG1 Fc-domain (shown in gray). The Fc-domain has been engineered to reduce interaction with FcγRs, thereby avoiding depletion of target cells by antibody-dependent cellular cytotoxicity/antibody-dependent cellular phagocytosis (ADCC/ADCP) or complement-dependent cytotoxicity (CDC) and restricting activation of 4–1BB only when simultaneously engaged to 5T4. **B,** The mode of action of ALG.APV-527: ALG.APV-527 directs the stimulation of T cells and NK cells to $5T4^{+}$ tumors and is designed to minimize the toxicity observed with other 4–1BB therapeutics. (i) ALG.APV-527 localizes to tumors where both targets, 4–1BB and 5T4, are highly expressed. (ii) ALG.APV-527 binds simultaneously to 5T4 on tumor cells and 4–1BB on tumor-infiltrating immune cells that activates the immune cells (e.g., enhances secretion of cytolytic molecules such as IFNγ and granzyme B and promotes proliferation). (iii) Activated immune cells induce cytolysis of tumor cells. **C,** X-ray structure of the parental 4–1BB–binding domain (Fab1618) in ribbon (blue) bound to 4–1BB (green shades, surface projection) showing that the binding epitope includes residues in domain 1 (lemon green) and domain 2 (forest green) of 4–1BB. Eleven hydrogen bonds were found between CDRH1 (yellow), CDRH2 (orange), CDRH3 (magenta), CDRL1 (red), and 4–1BB as shown in the close-up picture to the left. The 4–1BBL (trimeric 4–1BBL, in surface projection, light purple) binding to 4–1BB has been superimposed to illustrate the binding sites of ALG.APV-527, and the 4–1BBL on 4–1BB are distinct.

An extensive examination of the binding specificity of ALG.APV-527 was conducted using the Retrogenix cell microarray technology (Charles River Laboratories) to confirm target specificity to 5T4 and 4–1BB and rule out nonspecific off-target binding to other cell membrane and plasma-derived proteins. It was concluded that ALG.APV-527 binds specifically to both of its intended targets in the absence of off-target interactions (Supplementary Fig. S3E). All very weak, unrelated protein–binding interactions were ruled out based on SPR experiments or protein sequence homology searches.

### Agonistic effect of ALG.APV-527 on T and NK cells is 5T4 conditional

The ability of ALG.APV-527 to induce 5T4-conditional activation of 4–1BB was demonstrated using a 4–1BB/NFκB reporter cell assay.

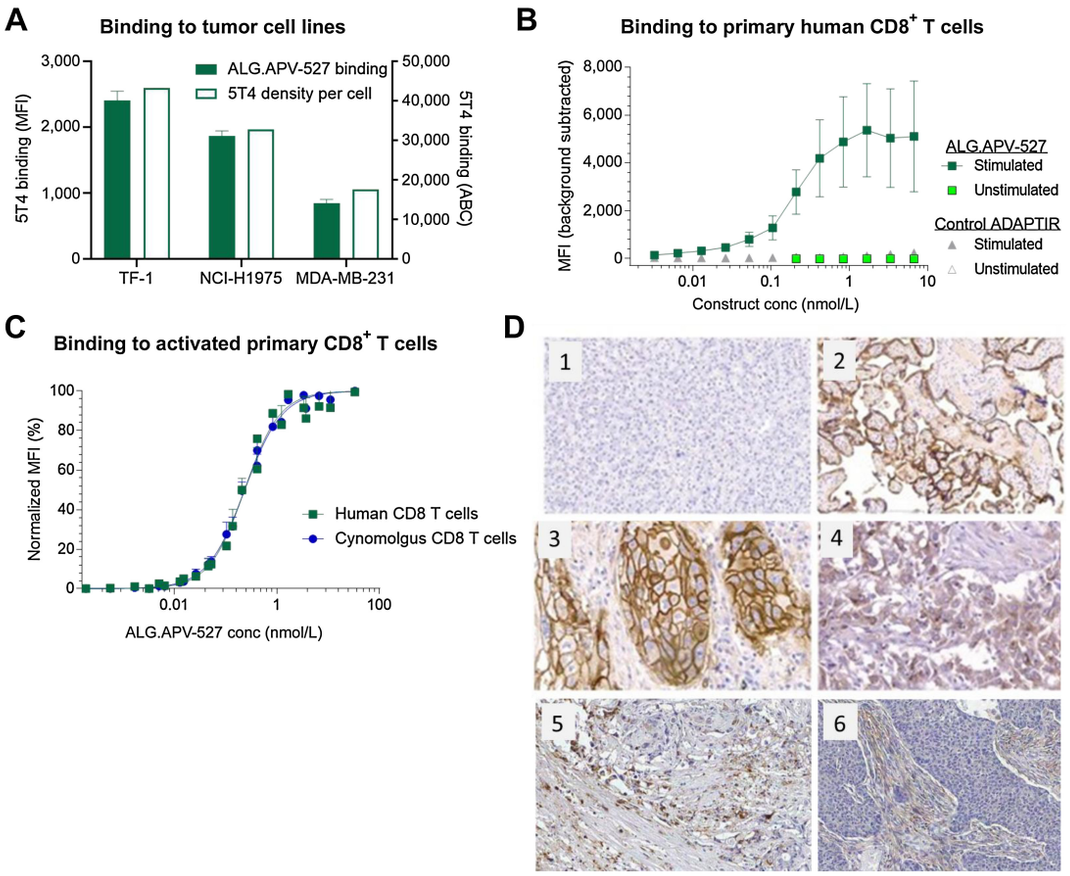


**Figure 2.**

ALG.APV-527 binding to target and target expression. **A,** Binding of ALG.APV-527 to human 5T4-expressing tumor cells using flow cytometry. Secondary fluorescently labeled Fc-targeting Ab was used for detecting bsAb binding and quantified using flow cytometry plotted at MFI. Quantification of 5T4 protein expression was done using BD Quantibrite beads. Antibodies bound per cell (ABC) were calculated using the lots' standard of PE molecules bound per cell. **B** and **C,** Primary human PBMCs were stimulated for 48 hours with or without α-CD3, biotinylated ALG.APV-527, or isotype ADAPTIR. Control was added in a serial dilution followed by streptavidin-APC and cell surface markers for T cells. Cells were then gated on $CD3^+CD8^+$ cells and analyzed for binding using flow cytometry and plotted as (**B**) MFI (background subtracted). **C,** Human and cynomolgus α-CD3–activated PBMCs were also plotted using nonlinear regression log (agonist) versus normalized response—variable slope. Data normalized pooled data from two experiments are shown, total $n = 6$. **D,** Formalin-fixed paraffin-embedded TMAs were stained for 5T4 expression. 5T4 expression was not detected in the liver (1). 5T4 expression was detected in the placenta (2; positive control) and in multiple tumor indications with variable incidence, frequency (percentage of positive cells), and intensity in staining (0–3+), as exemplified in images of NSCLC (3; 2–3+, >75%), malignant epithelial mesothelioma (4; 1–3+, >75%), pancreatic duct adenocarcinoma (5; 1–3+; >75%), and squamous cell carcinoma of the tongue (6; 1–3+ >50–75%).

The increase in 4–1BB activation depended on the presence of 5T4 (**Fig. 3A**, left), as there was no 4–1BB activation in the 5T4-negative cocultures (**Fig. 3A**, left center). In addition, ALG.APV-527 did not induce activity in the presence of the high-affinity human IgG FcγRI (CD64, **Fig. 3A** right center). In contrast, an urelumab analogue showed 4–1BB activity without crosslinking and was further enhanced with FcγR crosslinking (**Fig. 3A**). Moreover, ALG.APV-527 induced dose-dependent 4–1BB activity with human tumor cell lines expressing various levels of 5T4 (**Fig. 3A**, right).

ALG.APV-527 induced a dose-dependent expansion of CD8 T cells indicated by T-cell counts and fluorescent dye dilution, when incubated with CD3-stimulated PBMC cocultured with 5T4-expressing MDA-MB-231 tumor cells (**Fig. 3B**) or 5T4-engineered CHO cells (**Fig. 3C**). Of note, CD3-stimulation of PBMCs primarily upregulated 4–1BB expression on CD8 T cells (**Fig. 3D**). The ability of ALG.APV-527 to enhance activation of human T cells in the presence or absence of 5T4 was examined in PBMC cocultures using murine CT26-hu5T4 or CT26-WT. ALG.APV-527 augmented a dose-dependent increase in the frequency of CD8 and CD4 T cells expressing IFNγ only in the presence of 5T4-expressing cells (**Fig. 3E**). Expression of IFNγ was more frequent in the CD8 than in the CD4 T-cell population, which is consistent with the preferential expression of 4–1BB on CD8 T cells. Similarly, in purified CD8 T-cell assays, ALG.APV-527–induced IFNγ production was observed only in cultures with 5T4-expressing tumor cells, but not with 5T4-negative cells (**Fig. 3F**). Moreover, the presence of endogenous levels of 5T4 expressed on cocultured human HCT 116 tumor cells was enough to induce CD8 T-cell activation (**Fig. 3G**). The $EC_{50}$ value of ALG.APV-527 in human CD8 T-cell assays with 5T4-expressing cells ranged from 0.17 to 0.41 nmol/L. In addition, CD3-stimulated CD8 T cells upregulated the costimulatory receptor OX40 that was further enhanced with ALG.APV-527 stimulation (**Fig. 3H**).

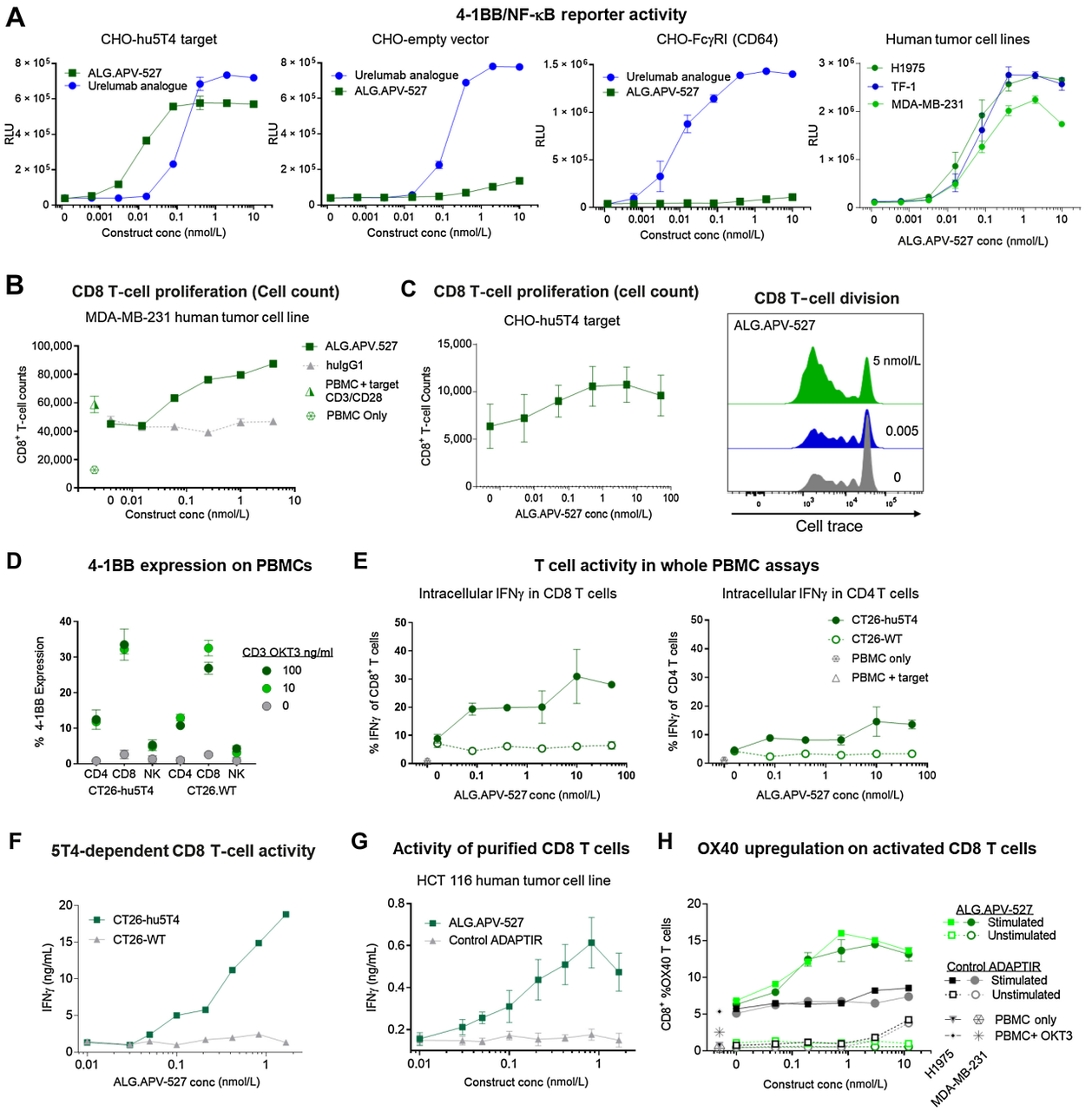


**Figure 3.**

Agonist function of ALG.APV-527 on T cells is dependent on 5T4 engagement resulting in T-cell activation and proliferation. **A,** 4–1BB reporter cells were stimulated with serial dilutions of ALG.APV-527 or urelumab analogue in the presence of hu5T4 (left), empty vector (left center) transfected CHO-K1 cells, FcγR1-tranfected CHO cells (right center) or different 5T4-expressing tumor cells (right) for 5 hours. The 5T4 receptor levels were evaluated on TF1 (17530/cell), H1975 (43153/cell), and MDA-MB-231 (32670/cell) using QuantiBright beads. **B,** PBMC were cocultured with MDA-MB-231 cells, 10 ng/mL OKT3, and a titration of ALG.APV-527 or huIgG1 controls for 6 days. The graphs show the number of CD8 T cells that had undergone at least one cell division and are represented as cell counts. **C,** Primary cell trace–labeled PBMCs were stimulated with α-CD3 Ab in solution and serial dilutions of ALG.APV-527 in the presence of 5T4-expressing CHO-K1 cells. The number of $CD8^+$ T cells (left) and a representation of the proliferation of $CD8^+$ T cells (right) were evaluated at 96 hours via flow cytometry. Average of three healthy donors is graphed. **D** and **E,** Primary PBMCs were stimulated with 0, 10 or 100 ng/mL of α-CD3 (OKT-3) in solution and serial dilutions of ALG.APV-527 in the presence of CT26-hu5T4 or CT26-WT cells for 48 hours. **D,** Expression of 4–1BB on CD4 T cells, CD8 T cells and NK cells. **E,** Intracellular IFNγ levels were evaluated using flow cytometry in CD8 T cells (left) or CD4 T cells (right). **F,** Purified T cells and sub-lethally UV-irradiated CT26-WT cells or CT26-hu5T4 tumor cells transfected to express 5T4 ($1\times10^6$/cell) were incubated with a dilution of ALG.APV-527. The secretion of IFNγ was measured in the supernatant after 72 hours of culture using ELISA. **G,** Purified CD8 T cells were co-cultured with HCT 116 tumor cells, α-CD3 (OKT-3) on beads, and serial dilutions of ALG.APV-527. IFNγ was assessed by ELISA. **H,** PBMCs were cultured with either MDA-MB-231 or H1975 tumor cell lines, α-CD3 OKT3 at 10 ng/mL and titrated ALG.APV-527, or the negative control ADAPTIR. OX40 surface expression was evaluated via flow cytometry at 72 hours.

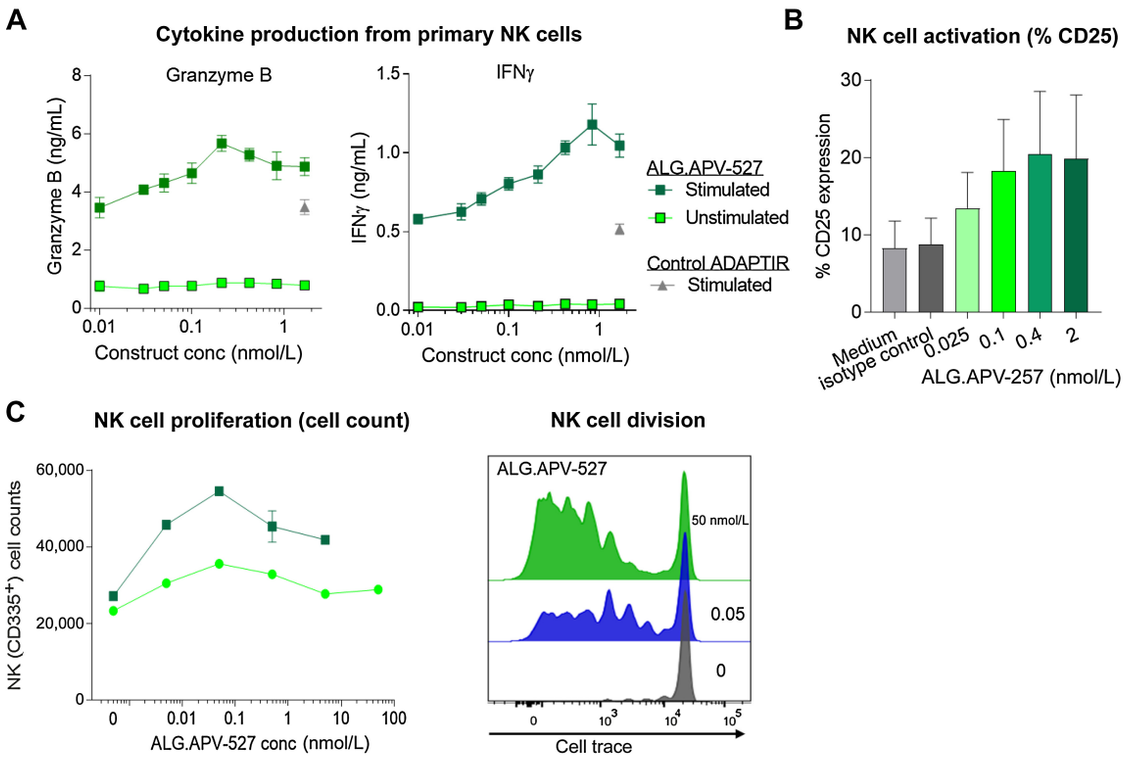


**Figure 4.**

ALG.APV-527 enhances NK cell activation and proliferation. **A** and **B,** Primary IL2-stimulated (10 ng/mL) NK cell assays and Mitomycin C–treated HCT116 tumor cells expressing endogenous levels of 5T4 ($6.2\times10^4$/cell) were incubated with a dilution of ALG.APV-527. **A,** The secretion of Granzyme B and IFNγ was measured in the supernatant after 72 hours of culture using ELISA. **B,** The expression of CD25 was measured by flow cytometry after 24 hours in culture. **C,** Primary NK cells were stimulated with IL2 (8 ng/mL) and serial dilutions of ALG.APV-527 in the presence of irradiated CHO-hu5T4 cells. The number of $CD335^+$ NK cells were assessed in 2 healthy samples on day 6 by flow cytometry (**C**, left) and representative dilution of CellTrace proliferation (**C**, right).

Moreover, ALG.APV-527 induced dose-dependent activation of IL2-stimulated NK cells, as measured by granzyme B, IFNγ (**Fig. 4A**), and CD25 expression (**Fig. 4B**). NK cells without IL2 prestimulation did not secrete granzyme B or IFNγ, supporting the premise that resting peripheral NK cells do not express 4–1BB and therefore, will not be augmented by ALG.APV-527 treatment. ALG.APV-527 also enhanced proliferation of IL2-stimulated NK cells as shown by both NK cell counts and CellTrace dilution (**Fig. 4C**).

Finally, the ability of ALG.APV-527 to enhance *in vitro* T-cell–mediated tumor cell killing in combination with a bsAb CD3 T-cell engager demonstrated enhanced tumor cell killing compared with ALG.APV-527 or the T-cell engager treatment alone (Supplementary Fig. S4A).

### ALG.APV-527 localizes to 5T4-expressing tumors, induces tumor-directed immune activation that eliminates growth of established tumors, and generates antitumor memory responses

Antigen-dependent tumor localization of ALG.APV-527 was evaluated in B16.WT/B16-hu5T4 twin tumor-bearing mice (outlined in **Fig. 5A**). An increase in ALG.APV-527 in 5T4-positive, but not in 5T4-negative tumors, was observed using IHC (**Fig. 5B**) and confirmed by flow cytometry using tumor single-cell suspensions (**Fig. 5C**).

The antitumor activity was assessed in hu4–1BB KI mice with established syngeneic MB49-hu5T4 tumors (outlined in **Fig. 5D**), in an initial study indicated a potent tumor killing at doses of 20 μg (Supplementary Fig. S4B). Further titration of ALG.APV-527 induced robust antitumor responses in doses as low as 2 μg (corresponding to 0.1 mg/kg, **Fig. 5E**) with sustained survival (**Fig. 5F**). Moreover, mice that had previously rejected MB49-hu5T4 tumors following ALG.APV-527 treatment were immune to rechallenge with either MB49-WT or MB49-hu5T4 tumors, in contrast with naïve mice, demonstrating the ability for ALG.APV-527 to promote the generation of immunological memory to a variety of tumor-specific antigens beyond hu5T4 (**Fig. 5G**).

### ALG.APV-527 does not induce peripheral systemic activation or toxicities in hu4–1BB KI mice or NHPs

Urelumab was among the first generation of 4–1BB mAbs, but has been shown to induce hepatotoxicity in clinical studies (22). Therefore, the *in vivo* immune-related effects of ALG.APV-527 were assessed in tumor-free hu4–1BB KI mice and compared with an urelumab analogue (outlined in **Fig. 6A**). Treatment with 200 μg/mouse ALG.APV-527 (corresponding to 10 mg/kg) was well tolerated with no treatment-related weight loss. In contrast, urelumab analogue-treated mice lost on average 7% of their pretreatment body weight (**Fig. 6B**) and developed dermatitis in seven of nine mice by visual examination, suggesting an improved tolerability of ALG.APV-527 compared with urelumab. At day 21, no significant difference in overall liver weight (Supplementary Fig. S5A) or any significant increases in serum liver enzymes

aspartate transaminase or alanine transaminase levels were observed in either treatment group compared with the IgG control (Supplementary Fig. S5B). Furthermore, there were no significant differences in spleen weight between the IgG control and ALG.APV-527–treated mice, whereas treatment with the urelumab analogue resulted in a significant increase in spleen weight (**Fig. 6C**). ALG.APV-527 had no effect on the frequency of proliferating T or NK cells in the spleen or blood, whereas the urelumab analogue induced significant increases in proliferating cells. The increase was observed in both CD8 (**Fig. 6D**) and CD4 T-cell subsets (Supplementary Fig. S5C) and in NK cells (Supplementary Fig. S5D).

Importantly, treatment with the urelumab analogue, but not ALG.APV-527, resulted in a significant mononuclear cell infiltration in the centrilobular region of the liver, which consisted of primarily CD8 T cells. In contrast, ALG.APV-527 treatment was associated with minimal, disperse immune cell infiltrates (**Fig. 6E**).

For justification of toxicology species, ALG.APV-527 was determined to be fully cross-reactive to cynomolgus macaques (**Fig. 2C**; Supplementary Fig. S3) and able to augment production of IFNγ by T cells similarly to human T cells *in vitro* (Supplementary Fig. S6A). A repeated dose GLP toxicology study in cynomolgus macaques (design in Supplementary Fig. S6B) demonstrated that five intravenous infusions of ALG.APV-527 given weekly at 5, 15, or 50.5 mg/kg were well tolerated with no ALG.APV-527–related clinical observations. There were no ALG.APV-527–related changes to clinical chemistry, hematology, coagulation or urinalysis test results and no adverse findings in ophthalmoscopy, macroscopic or microscopic assessment of tissues. No general elevation in liver enzymes or changes in liver histopathology were observed during treatment (Supplementary Fig. S6C). Limited safety pharmacology evaluations (electrocardiograms, blood pressure and respiratory rates) were performed in the GLP toxicology study, with no adverse effects in any parameters. The no observed adverse effect level (NOAEL) was the highest evaluated dose (50.5 mg/kg/wk) corresponding to a maximal concentration ($C_{max}$) of 1,200 μg/mL on day 1 (the highest $C_{max}$ of 1,880 μg/mL reached during the study was detected on day 22).

A generally dose-proportional increase in the levels of ALG.APV-527 detectable in blood confirmed exposure during the entire duration of the study in all dose groups. Analysis of the PK determined the serum half-life to be 5.1 to 9.5 days (Supplementary Fig. S6D and S6E), resulting in a predicted human half-life in the range of 10.8 to 26.9 days with a mean of 14 days.

## Discussion

4–1BB immunotherapies have the potential to address an important need in immuno-oncology and to provide additional clinical benefits in patients with checkpoint inhibitor refractory disease. Conditionally active bsAbs targeting 4–1BB and TAAs provide an opportunity to achieve an effective and safe treatment to overcome the limitations of the first-generation 4–1BB mAbs for solid tumor indications, including on-target crosslinking-independent hepatotoxicity (17). ALG.APV-527 targets the oncofetal antigen 5T4 that is expressed on multiple solid tumors, with limited to no expression on normal adult tissues. This is unlike other tumor antigens targeted by other 4–1BB bispecific molecules, such as HER2, which is expressed on epithelial cells in the gastrointestinal, respiratory, reproductive, and urinary tract as well as in the skin, breast, and placenta (23) or PD-L1, which is expressed by tissue resident immune cells, including Kupffer cells, and liver sinusoidal endothelial cells (24, 25). In addition, ALG.APV-527 mediates 4–1BB activation in cis, as defined by 4–1BB costimulation provided by the same cell that provides TCR activation (i.e., the tumor cell; ref. 26). This has been shown to be more effective than 4–1BB agonists that provide co-stimulation in trans, for example, those targeting tumor stroma via antigens such as FAP (26).

The unique 4–1BB–binding epitope of ALG.APV-527, as defined by X-ray crystallography, is located at the membrane distal end (domain 1 and 2) that does not block 4–1BBL binding. Although the epitope is located at the membrane distal end, it is clearly distinct from the urelumab-binding epitope. There is a complex interplay between the epitope and functional activity of 4–1BB antibodies, as well as with other members of the TNFRSF (19, 27). It may be speculated that binding to the membrane distal end of 4–1BB, while retaining crosslinking dependency, confers favorable properties in terms of stronger functional activity compared with 4–1BB binders that bind to a membrane proximal domain (such as utomilumab; ref. 19).

The requirement for 5T4-mediated crosslinking for biological effects was shown in multiple human functional assays. In all cases, 5T4 expression was required for ALG.APV-527–mediated 4–1BB costimulation. The $EC_{50}$ value of ALG.APV-527 in CD8 T-cell functional assays (0.17–0.41 nmol/L) is comparable with the published *in vitro* potency of urelumab (∼0.5–1 nmol/L) and more potent than utomilumab (∼10–20 nmol/L; refs. 19, 28, 29). Furthermore, the potency is in the same range as other tumor targeting 4–1BB bispecific drug candidates (30–32). These data, coupled with the requirement for 5T4 crosslinking for 4–1BB costimulatory activity and the potent *in vivo* activity of ALG.APV-527, have the potential to result in a favorable therapeutic index.

The activity of ALG.APV-527 was found to be stronger in CD8 T cells than CD4 T cells and correlated directly with a higher 4–1BB expression on CD8 versus CD4 T cells. These data support the preferential effect of ALG.APV-527, activating infiltrating tumor-specific CD8 T cells. The IHC-based 5T4 expression data presented here confirm reported data showing that 5T4 is mainly expressed in tumors with limited expression in normal healthy tissue (11–15). Tumor antigen–dependent drug localization was investigated in a mouse model, demonstrating that ALG.APV-527 can penetrate tumors, and localize to 5T4-expressing tumor cells.

In a bladder tumor model–expressing human 5T4, ALG.APV-527 induced strong antitumor effects. Cured mice rejected tumor rechallenge of both 5T4-positive and -negative tumors, demonstrating that ALG.APV-527 enables mice to develop a memory T-cell response for tumor antigens beyond 5T4. This clearly differentiates ALG.APV-527 from CD3-targeting T-cell engagers and tumor targeting antibody–drug conjugates that primarily kills TAA-positive tumor cells and require homogenous TAA expression to be efficacious, suggesting that ALG.APV-527 has the ability to mediate antitumor effects in tumors with heterogeneous 5T4 expression.

ALG.APV-527 was compared with an urelumab analogue in humanized 4–1BB mice for the appearance of liver histopathology and systemic immune cell activation and expansion. ALG.APV-527 did not elicit overt signs of toxicity, as mice treated at 200 μg (a dose 10- to 100-fold above than the efficacious dose in antitumor studies) did not display any weight loss or changes in splenic weight or cellularity. In contrast, urelumab, which is known to elicit hepatotoxicity, was poorly tolerated leading to weight loss, increases in splenic weight, and CD8 T-cell liver infiltration.

Administration of ALG.APV-527 was well tolerated in cynomolgus macaques and displayed no signs of adverse events at the highest dose assessed. Overall, the preclinical safety profile of ALG.APV-527

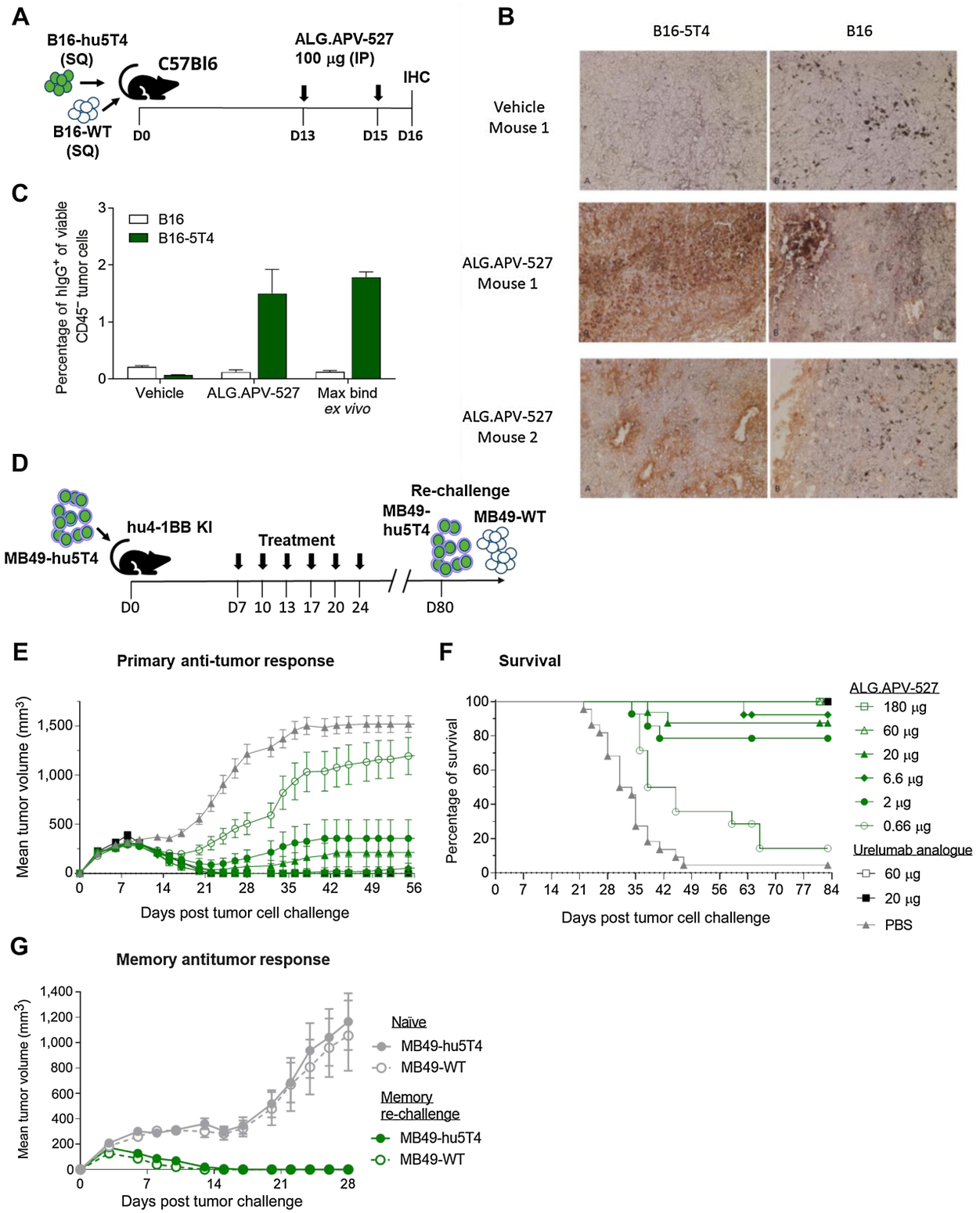

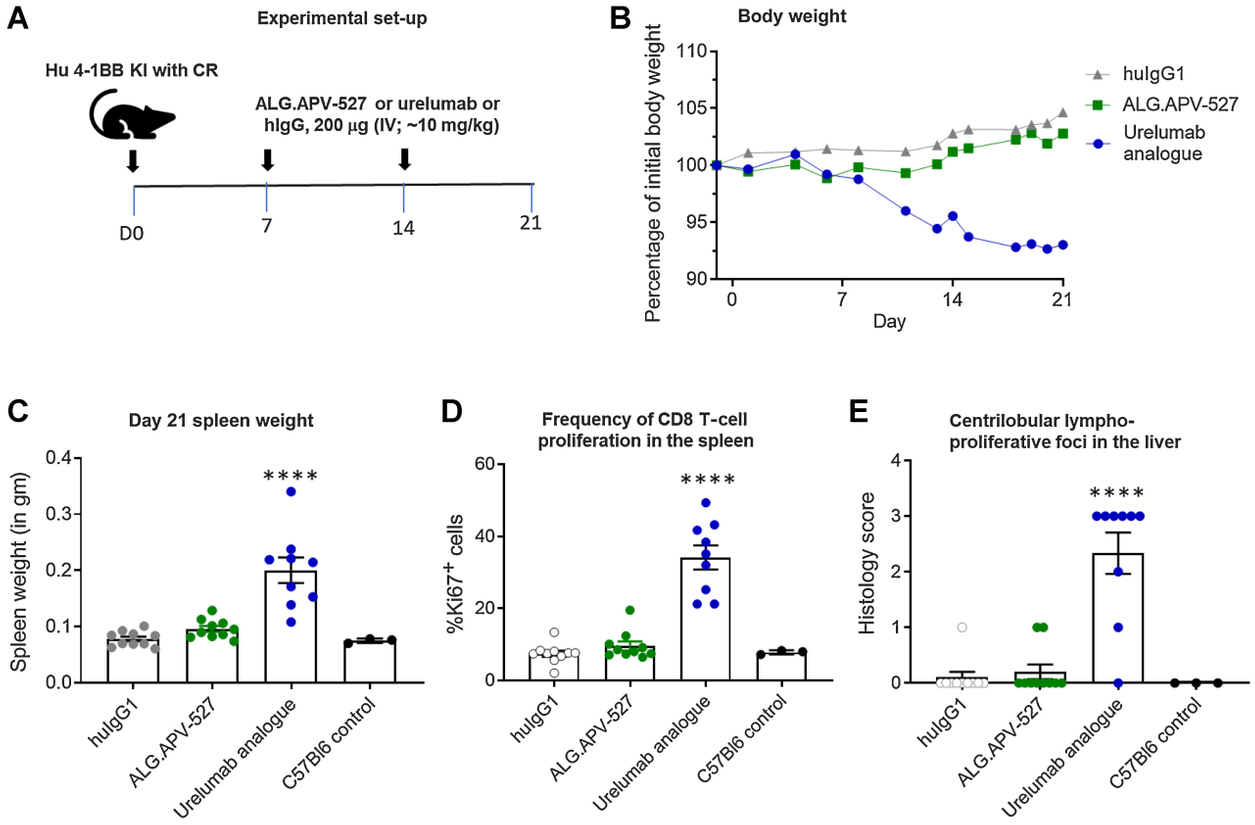


**Figure 6.**

ALG.APV-527 does not induce systemic immune activation *in vivo* in a human 4–1BB knockin mouse. **A,** Pharmacodynamic analysis. Hu4–1BB KI mice with that had a curative response to MB49-hu5T4 tumors, and therapy was used in this follow-up pharmacodynamic study. All mice previously on study were pre-bled before the start of this study and verified to have negative antidrug antibodies. A total of 200 μg of test reagent was given on days 0, 7, and 14 of the study. **B,** Body weight is plotted as the percentage of initial (day −1) for each group throughout study. **C,** On day 21 of the study, spleens were removed from euthanized mice and weighed. **D,** Treatment effects on splenic T-cell proliferation were evaluated via Ki67 staining. **E,** Treatment effects on liver inflammation was evaluated on hematoxylin and eosin–stained liver section. Sections were scored for infiltrates in centrilobular regions as well as lymphoproliferative foci and random inflammation by a blinded pathologist. The sections were scored for inflammation and assigned a score of 0, none; 1, minimal; 2, mild; 3, moderate; and 4, moderate with hepatocellular degeneration. Lymphoproliferative foci were scored 0, none or 1, present. Significant differences in end point measurements were determined using JMP one-way ANOVA analysis followed by the Tukey–Kramer HSD method for comparisons of all pairs. Differences between test items and controls that were statistically significant are marked in the figure with asterisks (*), where ****, $P < 0.0001$.

**Figure 5.**

ALG.APV-527 localizes to 5T4-expressing tumors *in vivo* and induces tumor rejection and memory responses. **A,** Twin tumor model experimental set-up: On day 0, each mouse received one 5T4-negative (B16.WT) and one 5T4-positive (B16-hu5T4) tumor injected (subcutaneous, $1\times10^5$ cells) at each side of the hind flank/back. Intraperitoneal treatment of ALG.APV-527 (100 μg) was given on days 6 and 13, and mice were sacrificed on day 14 (24 hours after the final treatment). Tumors were collected, and the level of binding of ALG.APV-527 to cells was assessed by IHC using an antibody-detecting human IgG. **B,** IHC images of ALG.APV-527 or vehicle control localized to 5T4-negative tumors (left) or 5T4-positive tumors (right). **C,** Detection of ALG.APV-527 binding to single-cell suspensions of 5T4-positive or -negative tumors using anti-human IgG by flow cytometry. The graph shows the mean frequency ± SEM of human $IgG^+$ cells among live $CD45^-$ tumor cells after two doses of ALG.APV-527 ($n = 5$). As control of maximal binding to the single-cell suspension, reagents (ALG.APV-527 and anti-human IgG) were also added *ex vivo* to only vehicle-treated mice ($n = 2$). **D,** Experimental set-up to assess antitumor efficacy and memory responses. **E** and **F,** Day 0, $4\times10^6$ MB49 cells expressing human 5T4 were injected subcutaneously into hu4–1BB KI mice. Starting on day 7, treatments of ALG.APV-527 or urelumab analogue were administered intraperitoneally twice weekly until day 24, and tumor volume and survival were assessed over time. Tumor volumes and survival from three studies were combined; $n = 8$–16 mice per group. The dose schedule was the same for all studies with treatments on days 7, 10, 13, 17, 20, and 24 post tumor challenge. **E,** Mean ± SEM of tumor volume for each group, pooled from the three separate studies is presented. For animals that reached tumor endpoints, that last recorded value was carried forward. **F,** Survival events were recorded each time a mouse reached the endpoint (tumor volume ≥1,500 $mm^3$). Pooled survival data from three studies are presented as median survival and statistical significance were calculated for the combined three studies using JMP survival analysis with a log-rank test and Wilcoxon test for comparison of survival curves. **G,** Complete responder mice that had cleared their primary tumors were re-challenged with $4\times10^6$ MB49–5T4 or $0.5\times10^6$ MB49-WT tumor cells on day 80. Naïve mice served as controls. No additional therapy was given. Seven to eight mice/treatment group. **E** and **G,** Mean tumor volume +SEM for each group is plotted until the first mouse in group reached the endpoint. Differences in mean tumor volume from day 3 through day 26 for the study groups were determined using JMP-repeated measures' analysis with the Tukey's multiple comparison test. All treatment groups ($P < 0.05$) were considered significant compared with controls.

indicates that it has the potential to effectively target 4–1BB without inducing liver toxicity (17).

In conclusion, the data presented here show that ALG.APV-527 has the potential to activate T cells and NK cells that are present in the TME in patients with various 5T4-expressing solid malignancies. The preclinical safety studies herein also suggest that ALG.APV-527 displays a wide therapeutic window. As there is an unmet need for therapies with the potential to improve response rates seen with checkpoint inhibitors in multiple cancer indications, these data provide support to advance ALG.APV-527 into clinical development.

## Authors' Disclosures

M.H. Nelson reports other support from Aptevo Therapeutics during the conduct of the study and other support from Aptevo outside the submitted work. S. Fritzell reports other support from Alligator Bioscience AB and grants from Vinnova during the conduct of the study, other support from Alligator Bioscience AB outside the submitted work, as well as a patent for WO 2019/016402 and WO 2017/182672 issued. D. Van Citters reports other support from APVO stock outside the submitted work and a patent for US20200223933A1 pending. A. Nilsson reports other support from Alligator Bioscience AB during the conduct of the study and other support from Alligator Bioscience AB outside the submitted work. L. Ljung reports other support from Alligator Bioscience outside the submitted work. R. Bader reports other support from Aptevo Therapeutics during the conduct of the study. A.G. Chunyk reports other support from Aptevo Therapeutics during the conduct of the study as well as other support from Alpine Immune Sciences outside the submitted work. L. Schultz reports other support from Alligator Bioscience AB outside the submitted work. L.A. Varas reports other support from Alligator Bioscience AB outside the submitted work as well as a patent for WO 2019/016402 and WO 2017/182672 issued. J. Gross reports personal fees and other support from Aptevo Therapeutics during the conduct of the study, other support from Aptevo Therapeutics outside the submitted work, reports a patent for WO 2019/016402 WO 2017/182672 issued, and is a consultant for Aptevo Therapeutics—Collaboration with Alligator BioSciences (other authors). P. Pavlik reports employment and is a share holder of Aptevo Therapeutics. N. Veitonmäki reports a patent for WO20161185016 pending. H.J. Ramos reports employment at and holds stock from Aptevo Therapeutics. A. Säll reports other support from Alligator Bioscience during the conduct of the study, other support from Alligator Bioscience outside the submitted work, and reports a patent for WO 2019/016402 and WO 2017/182672 issued. A. Dahlman reports other support from Alligator Bioscience AB during the conduct of the study other support from Alligator Bioscience AB outside the submitted work, and reports a patent for WO 2019/016402 issued to Alligator Bioscience AB and Aptevo Therapeutics. D. Bienvenue reports other support from Aptevo Therapeutics, Good Therapeutics, and Bonum Therapeutics outside the submitted work, reports patents for WO 2019/016402 and WO 2017/182672 issued. L. von Schantz reports grants from the Swedish Governmental Agency for Innovation Systems during the conduct of the study and reports a patent for WO 2019/016402 and WO 2017/182672 issued. C.J. McMahan reports other support from Aptevo Therapeutics and Aptevo Therapeutics outside the submitted work. P. Ellmark reports grants from Vinnova during the conduct of the study, other support from Alligator Bioscience outside the submitted work, and reports a patent for WO 2017/182672 and WO 2019/016402 issued. No disclosures were reported by the other authors.

## Authors' Contributions

**M.H. Nelson:** Conceptualization, data curation, formal analysis, supervision, visualization, methodology, writing–original draft, writing–review and editing. **S. Fritzell:** Conceptualization, data curation, formal analysis, supervision, visualization, methodology, writing–original draft, writing–review and editing. **R. Miller:** Formal analysis, investigation. **D. Werchau:** Formal analysis, investigation. **D. Van Citters:** Formal analysis, investigation. **A. Nilsson:** Investigation. **L. Misher:** Conceptualization, formal analysis, investigation. **L. Ljung:** Investigation. **R. Bader:** Formal analysis, investigation. **A. Deronic:** Formal analysis, investigation. **A.G. Chunyk:** Formal analysis, investigation, writing–review and editing. **L. Schultz:** Formal analysis, investigation, writing–review and editing. **L.A. Varas:** Formal analysis, supervision, investigation. **N. Rose:** Formal analysis, investigation. **M. Håkansson:** Formal analysis, investigation. **J. Gross:** Resources, supervision. **C. Furebring:** Resources, supervision. **P. Pavlik:** Data curation, formal analysis. **A. Sundstedt:** Formal analysis, investigation, writing–review and editing. **N. Veitonmäki:** Resources, supervision, investigation. **H.J. Ramos:** Data curation, formal analysis, writing–review and editing. **A. Säll:** Formal analysis, investigation. **A. Dahlman:** Formal analysis, investigation. **D. Bienvenue:** Conceptualization, data curation, supervision, methodology. **L. von Schantz:** Conceptualization, formal analysis, investigation, writing–review and editing. **C.J. McMahan:** Conceptualization, data curation, formal analysis, methodology. **M. Askmyr:** Investigation. **G. Hernandez-Hoyos:** Conceptualization, formal analysis, supervision, methodology, writing–review and editing. **P. Ellmark:** Conceptualization, formal analysis, supervision, writing–original draft, writing–review and editing.

## Acknowledgments

The X-ray crystallography study was supported by a Vinnova grant (diary number 2018–03295). We thank the extended Aptevo and Alligator team for their support in generating and reviewing data related to the ALG.APV-527 project. We acknowledge Diamond Light Source for time on Beamline I04 under proposal number in23282 and thank Beamline staff for help with data collection. We also would like to acknowledge our former colleague Rebeca Kovacic at SARomics Biostructures for help with the crystallization experiment.

The publication costs of this article were defrayed in part by the payment of publication fees. Therefore, and solely to indicate this fact, this article is hereby marked "advertisement" in accordance with 18 USC section 1734.

## Note

Supplementary data for this article are available at Molecular Cancer Therapeutics Online (http://mct.aacrjournals.org/).

Received July 12, 2022; revised September 16, 2022; accepted October 31, 2022; published first November 7, 2022.

## References

1. Sanmamed MF, Etxeberria I, Otano I, Melero I. Twists and turns to translating 4–1BB cancer immunotherapy. Sci Transl Med 2019;11:eaax4738.
2. Bartkowiak T, Curran MA. 4–1BB agonists: multi-potent potentiators of tumor immunity. Front Oncol 2015;5:117.
3. Vinay DS, Kwon BS. Therapeutic potential of anti-CD137 (4–1BB) monoclonal antibodies. Expert Opin Ther Targets 2015;20:361–73.
4. Chester C, Ambulkar S, Kohrt HE. 4–1BB agonism: adding the accelerator to cancer immunotherapy. Cancer Immunol Immunother 2016;65:1243–8.
5. Chen L. CD137 Pathway: immunology and diseases: Springer Science+Business Media, LLC; 2006.
6. Ye Q, Song D-G, Poussin M, Yamamoto T, Best A, Li C, et al. CD137 accurately identifies and enriches for naturally occurring tumor-reactive T cells in tumor. Clin Cancer Res 2014;20:44–55.
7. Sakellariou-Thompson D, Forget M-A, Creasy C, Bernard V, Zhao L, Kim YU, et al. 4–1BB agonist focuses CD8(+) tumor-infiltrating T-cell growth into a distinct repertoire capable of tumor recognition in pancreatic cancer. Clin Cancer Res 2017;23:7263–75.
8. Zhu Y, Chen L. CD137 as a biomarker for tumor-reactive T cells: finding gold in the desert. Clin Cancer Res 2014;20:3–5.
9. Houot R, Goldstein MJ, Kohrt HE, Myklebust JH, Alizadeh AA, Lin JT, et al. Therapeutic effect of CD137 immunomodulation in lymphoma and its enhancement by Treg depletion. Blood 2009;114:3431–8.
10. Driessens G, Kline J, Gajewski TF. Costimulatory and coinhibitory receptors in antitumor immunity. Immunol Rev 2009;229:126–44.
11. Southall P, Boxer G, Bagshawe K, Hole N, Bromley M, Stern P. Immunohistological distribution of 5T4 antigen in normal and malignant tissues. Br J Cancer 1990;61:89–95.

12. Hole N, Stern PL. Isolation and characterization of 5T4, a tumour-associated antigen. Int J Cancer 1990;45:179–84.
13. Hole N, Barton-Hanson N, Berwick S, Stern P. Human trophoblast glycoproteins defined by monoclonal antibody 1D2. Exp Cell Biol 1988;56:39–48.
14. Stern PL, Harrop R. 5T4 oncofoetal antigen: an attractive target for immune intervention in cancer. Cancer Immunol Immunother 2017;66:415–26.
15. Harper J, Lloyd C, Dimasi N, Toader D, Marwood R, Lewis L, et al. Preclinical evaluation of MEDI0641, a pyrrolobenzodiazepine-conjugated antibody–drug conjugate targeting 5T4. Mol Cancer Ther 2017;16:1576–87.
16. Harrop R, O'Neill E, Stern PL. Cancer stem cell mobilization and therapeutic targeting of the 5T4 oncofetal antigen. Ther Adv Vaccines Immunother 2019;7: 2515135518821623.
17. Segal NH, Logan TF, Hodi FS, McDermott D, Melero I, Hamid O, et al. Results from an integrated safety analysis of urelumab, an agonist anti-CD137 monoclonal antibody. Clin Cancer Res 2017;23:1929–36.
18. Chester C, Sanmamed MF, Wang J, Melero I. Immunotherapy targeting 4–1BB: mechanistic rationale, clinical results, and future strategies. Blood 2017; 131:49–57.
19. Chin SM, Kimberlin CR, Roe-Zurz Z, Zhang P, Xu A, Liao-Chan S, et al. Structure of the 4–1BB/4–1BBL complex and distinct binding and functional properties of utomilumab and urelumab. Nat Commun 2018;9:4679.
20. Neuber T, Frese K, Jaehrling J, Jäger S, Daubert D, Felderer K, et al. Characterization and screening of IgG binding to the neonatal Fc receptor. mAbs 2014; 6:928–42.
21. Wang W, Lu P, Fang Y, Hamuro L, Pittman T, Carr B, et al. Monoclonal antibodies with identical Fc sequences can bind to FcRn differentially with pharmacokinetic consequences. Drug Metab Dispos 2011;39:1469–77.
22. Bartkowiak T, Jaiswal AR, Ager CR, Chin R, Chen C-H, Budhani P, et al. Activation of 4–1BB on liver myeloid cells triggers hepatitis via an interleukin-27–dependent pathway. Clin Cancer Res 2018;24:1138–51.
23. Press MF, Cordon-Cardo C, Slamon DJ. Expression of the HER-2/neu proto-oncogene in normal human adult and fetal tissues. Oncogene 1990;5:953–62.
24. Wu K, Kryczek I, Chen L, Zou W, Welling TH. Kupffer cell suppression of $CD8^+$ T cells in human hepatocellular carcinoma is mediated by B7-H1/programmed death-1 interactions. Cancer Res 2009;69:8067–75.
25. Yarchoan M, Xing D, Luan L, Xu H, Sharma RB, Popovic A, et al. Characterization of the immune microenvironment in hepatocellular carcinoma. Clin Cancer Res 2017;23:7333–9.
26. Otano I, Azpilikueta A, Glez-Vaz J, Alvarez M, Medina-Echeverz J, Cortés-Domínguez I, et al. CD137 (4–1BB) costimulation of CD8(+) T cells is more potent when provided in cis than in trans with respect to CD3-TCR stimulation. Nat Commun 2021;12:7296.
27. Yu X, Chan HTC, Orr CM, Dadas O, Booth SG, Dahal LN, et al. Complex interplay between epitope specificity and isotype dictates the biological activity of anti-human CD40 antibodies. Cancer Cell 2018;33:664–75.
28. Jure-Kunkel MN, Calarota S, Girit E, Abraham R, Balimane P, Price K, et al. Functional characterization of fully human anti-CD137 antibodies. Cancer Res 2006;66:1117.
29. Fisher TS, Kamperschroer C, Oliphant T, Love VA, Lira PD, Doyonnas R, et al. Targeting of 4–1BB by monoclonal antibody PF-05082566 enhances T-cell function and promotes antitumor activity. Cancer Immunol Immunother 2012;61:1721–33.
30. Geuijen C, Tacken P, Wang LC, Klooster R, van Loo PF, Zhou J, et al. A human CD137xPD-L1 bispecific antibody promotes antitumor immunity via context-dependent T-cell costimulation and checkpoint blockade. Nat Commun 2021; 12:4445.
31. Hinner MJ, Aiba RSB, Jaquin TJ, Berger S, Dürr MC, Schlosser C, et al. Tumor-localized costimulatory T-cell engagement by the 4–1BB/HER2 bispecific antibody–Anticalin fusion PRS-343. Clin Cancer Res 2019;25: 5878–89.
32. Lakins MA, Koers A, Giambalvo R, Munoz-Olaya J, Hughes R, Goodman E, et al. FS222, a CD137/PD-L1 tetravalent bispecific antibody exhibits low toxicity and antitumor activity in colorectal cancer models. Clin Cancer Res 2020;26:4154–67.